Revisiting the Bulge-Halo Conspiracy II: Towards explaining its puzzling dependence on redshift

Francesco Shankar[1*], Alessandro Sonnenfeld[2,3,4], Philip Grylls[1], Lorenzo Zanisi[1,5], Carlo Nipoti[6], Kyu-Hyun Chae[7], Mariangela Bernardi[8], Carlo Enrico Petrillo[9], Marc Huertas-Company[10,11], Gary A. Mamon[12], Stewart Buchan[1]

1 *Department of Physics and Astronomy, University of Southampton, Highfield, SO17 1BJ, UK*
2 *Kavli IPMU (WPI), UTIAS, The University of Tokyo, Kashiwa, Chiba 277-8583, Japan*
3 *Physics Department, University of California, Santa Barbara, CA 93106, USA*
4 *Physics and Astronomy Department University of California Los Angeles CA 90095-1547*
5 *Dipartimento di Fisica, Universitá di Roma "La Sapienza", P.le Aldo Moro 2, 00185, Roma, Italy*
6 *Department of Physics and Astronomy, Bologna University, via Gobetti 93/2, I-40129 Bologna, Italy*
7 *Department of Physics and Astronomy, Sejong University, 209 Neungdong-ro Gwangjin-Gu, Seoul 05006, Korea*
8 *Department of Physics and Astronomy, University of Pennsylvania, 209 South 33rd St, Philadelphia, PA 19104*
9 *Kapteyn Astronomical Institute, University of Groningen, Postbus 800, 9700 AV, Groningen, The Netherlands*
10 *LERMA, Observatoire de Paris, CNRS, Université Paris Diderot, Paris Sciences et Lettres (PSL) Research University, Université*
11 *Université Paris Denis Diderot, 75205 Paris Cedex 13, France*
12 *Institut d'Astrophysique de Paris (UMR 7095: CNRS & UPMC, Sorbonne Universités), 98bis Bd Arago, F-75014 Paris, France*

ABSTRACT

We carry out a systematic investigation of the total mass density profile of massive ($\log M_{\rm star}/M_\odot \sim 11.5$) early-type galaxies and its dependence on redshift, specifically in the range $0 \lesssim z \lesssim 1$. We start from a large sample of SDSS early-type galaxies with stellar masses and effective radii measured assuming two different profiles, de Vaucouleurs and Sérsic. We assign dark matter haloes to galaxies via abundance matching relations with standard ΛCDM profiles and concentrations. We then compute the total, mass-weighted density slope at the effective radius γ', and study its redshift dependence at fixed stellar mass. We find that a necessary condition to induce an increasingly flatter γ' at higher redshifts, as suggested by current strong lensing data, is to allow the intrinsic stellar profile of massive galaxies to be Sérsic and the input Sérsic index n to vary with redshift as $n(z) \propto (1+z)^\delta$, with $\delta \lesssim -1$. This conclusion holds irrespective of the input $M_{\rm star}$-$M_{\rm halo}$ relation, the assumed stellar initial mass function, or even the chosen level of adiabatic contraction in the model. *Secondary* contributors to the observed redshift evolution of γ' may come from an increased contribution at higher redshifts of adiabatic contraction and/or bottom-light stellar initial mass functions. The strong lensing selection effects we have simulated seem not to contribute to this effect. A steadily increasing Sérsic index with cosmic time is supported by independent observations, though it is not yet clear whether cosmological hierarchical models (e.g., mergers) are capable of reproducing such a fast and sharp evolution.

Key words: cosmology: theory – galaxies: evolution – galaxies: fundamental parameters

1 INTRODUCTION

The details of the evolution of the most massive galaxies are still a matter of debate. One of the most promising scenarios is the so-called two-phase evolutionary sequence, in which a fraction of the stars is created "in-situ", and the rest forms "ex situ" and is accreted at later times. It is however still quite debated what the relative contribution actually is between the fraction of stars formed in the initial burst of star formation, and the fraction of stars acquired on cosmological timescales via, e.g., mergers and/or cosmic flows (e.g., Cirasuolo et al. 2005; Lapi et al. 2006; Shankar et al. 2006; De Lucia & Blaizot 2007; Hopkins et al. 2008; Dekel et al. 2009; Naab et al. 2009; Oser et al. 2010; Shankar et al.

* E-mail: F.Shankar@soton.ac.uk

2010b,a; González et al. 2011; Lapi et al. 2011; Hirschmann et al. 2013; Shankar et al. 2013; Aversa et al. 2015; Buchan & Shankar 2016).

Valuable additional observational constraints on the evolutionary patterns of massive galaxies are derived from the structural evolution across cosmic time and galaxy properties. In particular, thanks to a variety of data from strong lensing and stellar dynamics, the last decade has seen a dramatic boost in the interest towards the "total" mass density profile of massive galaxies. The latter, on average well approximated by a power-law $\rho(r) \propto r^{-\gamma}$ with slope $\gamma \approx 2$ (see, e.g., Treu & Koopmans 2004; Koopmans et al. 2006; Gavazzi et al. 2007; Koopmans et al. 2009; Barnabè et al. 2011), has revealed clear trends with stellar mass, effective radius, and redshift (e.g., Auger et al. 2010; Ruff et al. 2011; Bolton et al. 2012; Sonnenfeld et al. 2013; Dye et al. 2014; Tortora et al. 2014a,b). The slope decreases for increasing galaxy size at fixed stellar mass, and for lower mass galaxies at fixed effective radius.

Building on previous work (e.g., Newman et al. 2013; Dutton & Treu 2014; Newman et al. 2015), Shankar et al. (2017b, paper I, hereafter) devised accurate semi-empirical models to create advanced mock galaxy catalogues based on a large galaxy sample with measured effective radii and stellar masses, together with basic assumptions on their host dark matter haloes (abundance matching). By varying the stellar mass profile, stellar initial mass function (IMF), stellar mass-halo mass relation, they concluded that the observed variations of the mass density slope with galaxy properties is naturally explained by the interplay between the combined stellar and halo profiles, with a preference for heavy stellar IMFs, and for uncontracted dark matter halo profiles as those expected from dark matter-only cosmological N-body simulations, at least for galaxies not in cluster environments.

Regarding cosmic time evolution, in particular, the total mass density slope has been observed to anti-correlate with redshift, being shallower for higher-redshift objects with respect to local systems of the same mass and size (e.g., Ruff et al. 2011; Bolton et al. 2012; Sonnenfeld et al. 2013; Dye et al. 2014). Explaining this trend is the focus of this second paper in the series. As the total mass density distribution is the sum of the density distributions of the stars and of the dark-matter halo, its gradual variation along cosmic time is expected to encode important clues on the relative evolution of these two components. In turn, being able to identify the key assumptions in the semi-empirical models that can best reproduce the observational data will shed light on the relative roles played by different processes in shaping galaxies. For example, if (dry) mergers are truly gradually growing the sizes of galaxies at late epochs, then one would naively expect somewhat *steeper* values of γ for higher-redshift, more compact, massive galaxies, a trend which could be directly tested in our semi-empirical models.

The structure of this work is the following. In Section 3 we briefly recap the semi-empirical model used to construct mock samples of galaxies. In Section 4 we present a series of models of the total mass density slope as a function of redshift, mainly focused on variations of the Sérsic index and stellar IMF and dark matter fractions, which we compare with strong lensing observations. In Section 5 we discuss our results in view of evolution of the mass density slope

along the putative progenitors and other issues of interest, and conclude in Section 6.

In the following we will adopt a reference cosmology with parameters $\Omega_{\rm m} = 0.30$, $\Omega_{\rm b} = 0.045$, $h = 0.70$, $\Omega_\Lambda = 0.70$, $n = 1$, and $\sigma_8 = 0.8$, to match those usually adopted in the observational studies on the stellar mass function and strong lensing considered in this work.

2 THE DATA

Observations of the total mean mass density slope γ' are taken from the gravitational strong lensing analysis of Sonnenfeld et al. (2013). The latter combined strong lensing and stellar kinematics data for 84 lens galaxies in the redshift interval $0.1 < z < 1$. They constrained the density slope of each object by fitting a spherical power-law density profile to the observed Einstein radius and central velocity dispersion. The model velocity dispersion was computed by solving the spherical Jeans equation under the assumption of isotropic orbits. Sonnenfeld et al. (2013) then fitted for the distribution of the slope γ' across the population of lenses. They described the distribution of γ' as a Gaussian with a mean that is a function redshift, stellar mass and size, given by

$$\langle \gamma' \rangle = \gamma_0 + \alpha(z - 0.3) + \beta(\log M_{\rm star} - 11.5) + \xi \log(R_{\rm e}/5),$$
(1)

with $\gamma_0 = 2.08^{+0.02}_{-0.02}$, $\beta = 0.40^{+0.16}_{-0.15}$, and $\xi = -0.76^{+0.15}_{-0.15}$, with an average dispersion around the median of $\sigma_{\gamma'} = 0.12^{+0.02}_{-0.02}$.

Effective radii of the lens galaxies were obtained by fitting de Vaucouleurs profiles. Stellar masses were measured through stellar population synthesis, using de Vaucouleurs magnitudes as input, and assuming a Salpeter IMF. Of particular relevance to this work, the constrained value for the redshift evolution parameter $\alpha = -0.31^{+0.09}_{-0.10}$, at face value would imply that, at fixed stellar mass and effective radius, a null evolution of γ' with redshift is rejected at $\gtrsim 3\sigma$ level. This trend with redshift was also anticipated by Bolton et al. (2012) and Ruff et al. (2011), and later also confirmed by Dye et al. (2014) who, analyzing five lens systems in the range $0.22 < z < 0.94$, concluded that the logarithmic slope of the total mass density profile steepens with decreasing redshift. Dye et al. (2014) also support a decreasing γ' with increasing effective radius at fixed redshift, in full agreement with equation 1 (and the modelling put forward in paper I).

To create the mock galaxy catalogue to compare to the Sonnenfeld et al. (2013) strong lensing data, we start from the Meert et al. (2015) sample extracted from the Sloan Digital Sky Survey (SDSS) DR7 spectroscopic sample (Abazajian et al. 2009) in the redshift range $0.05 < z < 0.2$, and with a probability $P(E) > 0.85$ of being elliptical galaxies based on the Bayesian automated morphological classifier by Huertas-Company et al. (2011). For this SDSS subsample we have at our disposal three different light profiles, a pure de Vaucouleurs (de Vaucouleurs 1948), a Sérsic+Exponential, and a pure Sérsic (Sérsic 1963) profile (see, e.g., Bernardi et al. 2013, 2017b). Slightly more accurate mass-to-light ratios from (Mendel et al. 2013) have been adopted for this sample with respect to those considered in paper I, which were based on Bell et al. (2003). We verified that all the

relevant scaling relations in terms of (de Vaucouleurs) stellar mass, size, and velocity dispersion are in equally good, if not even improved, agreement to the Sonnenfeld et al. (2013) sample.

To probe for a possible redshift evolution of the total galaxy mass density profiles, we will create redshift-dependent mock galaxy catalogues starting from our $z < 0.2$ SDSS galaxy sample and include some structural evolution in their light profiles as inspired by observational results. This is a safe approximation given that the number densities and morphological mix of galaxies have a weak dependence on redshift up to $z \lesssim 1$ (see, e.g., Huertas-Company et al. 2015, their Fig. 3). In what follows we will thus always assume that the effective radii of massive galaxies decrease with increasing redshift as $R_e \propto (1 + z)^{-1}$ at fixed stellar mass, in line with a number of independent observations of massive galaxies at high redshifts (e.g., Cimatti et al. 2012; Huertas-Company et al. 2013; van der Wel et al. 2014, and references therein). To isolate the redshift evolution in γ' from its dependence on stellar mass and effective radius, which we have already extensively explored in paper I, in Section 4 we will mostly focus on galaxies in very narrow bins of (de Vaucouleurs) stellar mass $11.4 < \log M_{\rm star} < 11.6$ and corresponding effective radii at $z \lesssim 0.1$ in the range $4 < R_e/{\rm kpc} < 6$. These represent the characteristic masses and sizes of typical galaxies in the reference observational sample of Sonnenfeld et al. (2013), as also evident from equation 1.

The main difference between this work and paper I is that in the latter we varied the assumed *intrinsic* stellar profile of our mock galaxies according to the choice of light profile adopted in the observational sample we were comparing with, i.e., de Vaucouleurs when comparing with Sonnenfeld et al. (2013) and Sérsic when comparing with Newman et al. (2013, 2015). Here we further expand on this methodology by distinguishing between an intrinsic and observed profile, with the former being what we believe is a more realistic modelling of the stellar profile of typical massive galaxies, and the latter being the actual one assumed in the observational sample used to compare the models with. In this logic, stellar masses and effective radii in this work will always be quoted as de Vaucouleurs quantities, as we will only compare to Sonnenfeld et al. (2013), but the intrinsic ones will vary from de Vaucouleurs to Sérsic profiles.

3 THE SEMI-EMPIRICAL MODEL

We here briefly describe the main features of the semi-empirical model adopted in this work, leaving the full details to paper I, and mostly highlighting the relevant differences/improvements with respect to it.

The nearly-isothermal total mass density profile inferred from strong lensing and stellar dynamics (e.g., Mamon & Łokas 2005b; Sonnenfeld et al. 2013; Cappellari et al. 2015) is believed to be a result of the combined steeper and flatter mass density profiles of, respectively, the stellar and dark matter components (known as the "bulge-halo conspiracy"). As extensively discussed in paper I, the relative contributions of these components within scales comparable to the half-mass radii of the galaxies should then dictate the

relative trends of the mass density slope with large-scale galaxy properties such as stellar mass and effective radius.

In our galaxy mocks, halo masses are assigned to each galaxy in our SDSS sample via abundance matching techniques. More precisely, at any redshift of interest we compute the mean relation between stellar mass and host halo mass via the equality between the cumulative stellar and (sub)halo mass functions

$$\Phi(> M_{\rm star}, z) = \Phi_h(> M_{\rm halo}, z). \qquad (2)$$

We include, throughout, a scatter of 0.15 dex in stellar mass at fixed halo mass constant with halo mass and redshift, a good approximation at these mass scales and at redshifts $z \lesssim 1$ (e.g., Shankar et al. 2014a). We incorporate scatter in the abundance matching by refitting the high mass-end slope of the scatter-free $M_{\rm star}$-$M_{\rm halo}$ relation (equation 9 in paper I) until it matches the input stellar mass function. As detailed in paper I we then invert the $M_{\rm star}$-$M_{\rm halo}$ relation by self-consistently computing the implied mean and scatter in halo mass as a function of stellar mass.

For the dark matter component in the right-hand side of equation 2 we adopt the host halo mass function of Tinker et al. (2008), with (unstripped) subhalo correction from Behroozi et al. (2013). Halo masses $M_{\rm halo}$ are always defined within r_{200c}, such that the average density within r_{200c} is 200 times the critical density of the Universe at redshift z. We always assume a Navarro et al. (1997) profile which, as proven in paper I, is a good approximation for (central) galaxies at the mass scale $\log M_{\rm star}/M_\odot \sim 11.5$ of interest to this work. The concentration-halo mass relation is taken from Diemer & Kravtsov (2015) with a log-normal scatter of 0.16 dex. We also consider NFW profiles modified by the inclusion of adiabatic contraction or adiabatic expansion following the methodology outlined by, e.g., Dutton et al. (2007) and Barausse (2012). Briefly, the final and initial radius of the mass distribution are related by the expression $r_f = \Gamma^\nu r_i$, with Γ the contraction factor (Blumenthal et al. 1986), and the parameter ν taking on the values $\nu = 0, 0.8, -0.3$ for no contraction, adiabatic contraction, and adiabatic expansion, respectively (full details in paper I).

For the stellar component on the left-hand side of equation 2 we rely on the Bernardi et al. (2017b) stellar mass function. The latter has a specific shape which we self-consistently vary according to the assumed stellar profile (de Vaucouleursor Sérsic), and/or assumed IMF (see below), before applying equation 2. Sérsic-based profiles tend to produce substantially higher number densities of massive galaxies and thus steeper $M_{\rm star}$-$M_{\rm halo}$ relations via equation 2 (see, e.g., Fig. 1 in paper I). For the remainder of this paper we assume each rendition of the Bernardi et al. (2017b) stellar mass function to be strictly constant in the redshift range $0 < z < 1$. Forcing a constant number density of massive galaxies up to $z \sim 1$ may be an oversimplification. Recent abundance matching and clustering modelling tends, in fact, to favour some stellar mass growth in the most massive galaxies (Buchan et al. 2017, submitted). This in turn would necessarily induce some late evolution in the high mass-end of the stellar mass function, thus impacting the exact shape of the implied stellar mass-halo mass relation (e.g., Kravtsov et al. 2014; Shankar et al. 2014a; Skibba et al. 2014; Coupon et al. 2015; Patel et al. 2015; Rodríguez-Puebla et al. 2015; Shan et al. 2015). As further discussed

below, however, the exact choice of input stellar mass function and/or $M_{\rm star}$-$M_{\rm halo}$ relation does not alter any of our conclusions, in the redshift range $0 < z < 1$. This is mainly because the dark matter fraction within the effective radius in massive galaxies remains relatively contained to $\lesssim 40\%$ even at high redshifts (see, e.g., Wojtak & Mamon 2013; Shetty & Cappellari 2015, and Section 4.3), coupled to a steep central stellar profile.

For each light profile we explore the impact of varying the input IMF, from a Chabrier (Chabrier 2003), the reference one adopted by Bernardi et al. (2017b), to a Salpeter (Salpeter 1955), and variable (velocity dispersion-dependent) IMF. For the former, we simply add 0.25 dex to each stellar mass (Bernardi et al. 2010). For the latter, we follow Cappellari et al. (2015) and Cappellari (2016, their Fig. 19), and express the variation in mass-to-light ratio with respect to Salpeter as

$$\log{(M/L)}\,[\sigma_e] = \log{(M/L)}_{\rm Salp} + {\rm f}(\sigma_e) =$$
$$\log{(M/L)}_{\rm Salp} - 0.0576 + 0.364 \times \log\left(\frac{\sigma_e}{200~{\rm km\,s^{-1}}}\right) \quad (3)$$

with an intrinsic scatter of 0.11 dex. We note that in this paper we will mainly focus on galaxies with stellar masses peaked around $\log M_{\rm star}/M_\odot \sim 11.5$ (Salpeter IMF), for which equation 3 yields stellar masses ~ 0.20 dex higher than a Chabrier IMF. We will thus not be able to fully probe the validity of equation 3 to all stellar masses, though we will be able to discern if a **heavy** IMF as the one given in is more appropriate than a Chabrier IMF in matching the data. We will also consider a model characterized by a variable IMF as in equation 3, which gradually tends towards a Chabrier IMF linearly with redshift as

$$\log{(M/L)}\,[\sigma_e, z] = \log{(M/L)}_{\rm Chab} + [0.25 + {\rm f}(\sigma_e)]\,(1 - z) \quad (4)$$

where we have assumed that a Chabrier IMF induces 0.25 dex lower stellar masses than a Salpeter IMF (e.g., Bernardi et al. 2010). equation 4 clearly reduces to equation 3 at $z = 0$. We note that the gradual transformation with redshift proposed in equation 4, even though possibly not fully aligned with other proposals in the literature (see, e.g., Sonnenfeld et al. 2017), is the only one still acceptable by our semi-empirical modelling, as it will become apparent in Section 4.2. A series of studies in recent years have also suggested that the IMF of massive early-type galaxies should be heavier in the centre and lighter in the outskirts (Martín-Navarro et al. 2015a,c; La Barbera et al. 2016; Conroy et al. 2017; van Dokkum et al. 2017). Following van Dokkum et al. (2017), for completeness we also present a model with a scale-dependent IMF parameterized[1] as

$$\Theta\,[R/R_e] = \begin{cases} \log[2.23 - 3.6(R/R_e)], & \text{if } R/R_e < 0.4 \\ 0, & \text{otherwise} \end{cases} \quad (5)$$

where $\Theta\,[R/R_e] = \log{(M/L)}\,[R/R_e] - \log{(M/L)}_{\rm MW}$. We

[1] We note that the normalization of equation 5 has been reduced by $\sim 10\%$, still within the range allowed by van Dokkum et al. (2017)'s data. Any higher normalization would further exacerbate the poor match between this model and the data reported in Fig. 2. Also, equation 5 has been strictly derived as a function of *projected* radii, though we will here simply extend it to 3D mass density distributions.
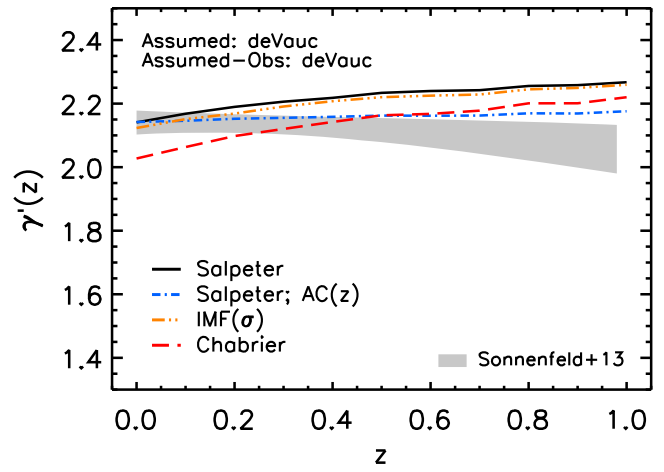

Figure 1. Predicted redshift evolution of the slope of the total mean mass density profile, measured at the effective radius, γ', for galaxies with stellar masses in the narrow interval $11.4 < \log M_{\rm star}/M_\odot < 11.6$ and effective radius at $z \leqslant 0.1$ in the range $4 < R_e(z)/{\rm kpc} < 6$, steadily decreasing proportionally to $(1+z)^{-1}$ at higher redshifts. All models assume an intrinsic de Vaucouleurs profile, as in the observations, and a $\propto (1+z)^{-1}$ redshift evolution in the effective radius R_e, but different IMFs, as labelled. The orange, triple dot-dashed line also includes an increasing adiabatic contraction towards higher redshifts (see text for details). Models are compared with data from Sonnenfeld et al. (2013) (grey band).

verified that equation 5 implies an average increase in stellar mass with respect to a Milky Way-type IMF (Kroupa 2001) of ~ 0.04 dex, with negligible dependence on stellar mass or effective radius. We then further add 0.05 dex to convert from a Kroupa (Kroupa 2001) to our reference Chabrier IMF (e.g., Bernardi et al. 2010).

Finally, for each galaxy in our mock we compute the mass-weighted slope of the total density profile within a radius r (Dutton & Treu 2014)

$$\gamma'(r) \equiv -\frac{1}{M(<r)}\int_0^r \frac{d\log\rho}{d\log x}4\pi x^2\rho(x)dx =$$
$$= 3 - \left.\frac{d\log{\rm M}}{d\log x}\right|_{x=r}. \quad (6)$$

Sonnenfeld et al. (2013, cfr. their Fig. 6) and Dutton & Treu (2014) have shown that the mass-weighted slope γ' computed within the effective radius R_e, is a good proxy of γ' derived from strong lensing and dynamical measurements (see Sonnenfeld et al. 2013, for a full discussion). In each model γ' will be self-consistently computed at the de Vaucouleurs effective radius, though we note that γ' has anyway a very weak dependence on scale within the range $(0.5-1.2)R_e$. Measuring γ' at, say, the Sérsic effective radius instead, which could be up to a factor of $\lesssim 2$ higher than the de Vaucouleurs effective radius (cfr. Fig. 1 in paper I), could induce an appreciable systematic drop of $\lesssim 10\%$ in the predicted γ'. However, this would, if anything, exacerbate the tensions between model predictions and data.
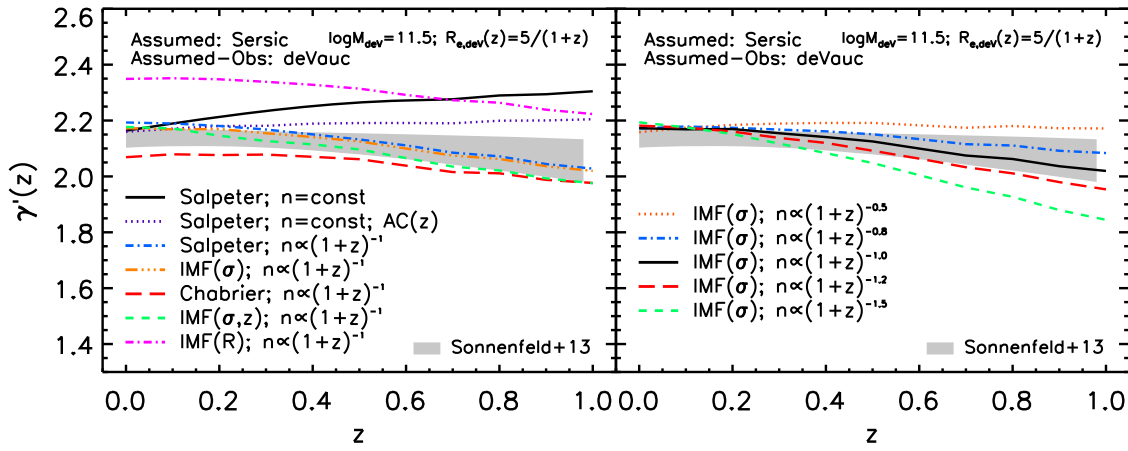
Figure 2. Same format as Fig. 1. Left: Comparison of models that assume an intrinsic Sérsic stellar profile and observed de Vaucouleurs stellar profile, a $(1 + z)^{-1}$ redshift evolution in the effective radius R_e, but different IMFs, as labelled. The purple, dot-dashed line also includes an increasing adiabatic contraction towards higher redshifts (see text for details). Right: Comparison of models with intrinsic Sérsic stellar profile and different degree of redshift evolution in the Sérsic index, as labelled. Only models with strong redshift evolution in the Sérsic index, $n \propto (1 + z)^{-\delta}$ with $\delta \gtrsim 0.7$, can broadly line up with the data.

4 RESULTS

4.1 Constraints on the stellar profile: An evolving Sérsic index

Fig. 1 shows[2] the predicted evolution in γ' for galaxies in very narrow bins of (de Vaucouleurs) stellar mass $11.4 < \log M_{\rm star} < 11.6$ and effective radius at $z = 0.1$ of $4 < R_e(z)/{\rm kpc} < 6$, steadily decreasing proportionally to $(1 + z)^{-1}$ at higher redshifts. A number of variants are reported in Fig. 1, with models characterized by a Salpeter, a variable, and a Chabrier IMF, as labelled. The grey area in Fig. 1 represents the median and 68% percentiles of the full posterior probability distribution of γ' inferred by Sonnenfeld et al. (2013) for galaxies at fixed stellar mass and redshift-dependent size. More precisely, at each redshift of interest we evaluate γ' from equation 1 for $\log M_{\rm star}/M_\odot = 11.5$ and $R_e(z) = 5/(1 + z)$ kpc, propagating the uncertainties on the parameters α and γ_0. The resulting γ' appears rather constant, or at most slightly flattening, with increasing redshift. This behaviour is expected from equation 1 which predicts a substantial decrease of γ' at higher redshifts, partly compensated by the steep (inverse) dependence on effective radius, the latter assumed to steadily decrease at earlier cosmic epochs.

As anticipated above, we choose very narrow intervals of stellar mass and effective radius for both the models and the data to highlight the dependence on redshift. It is important to stress that none of the main results discussed in this Section relies on the exact choice of bins in stellar mass and/or effective radius chosen for the analysis, as long as the same selections are self-consistently applied to both the models and the strong lensing data (via equation 1).

In line with what inferred in paper I, we confirm that

---

[2] To be fully consistent with paper I, specifically for Fig. 1 (only!), we continue adopting the mass-to-light ratio of Bernardi et al. (2013), and a de Vaucouleurs+Exponential (the so-called "cmodel" magnitudes) total stellar mass function to include in the abundance matching.

when comparing with the Sonnenfeld et al. (2013, grey band) data at $z \lesssim 0.2$, a Chabrier IMF appears to be disfavoured with respect to a variable or Salpeter IMF. What is new and more relevant to this specific work, is that all models predict at earlier cosmic epochs a flat, if not even slightly increasing, γ'. This (constant) behaviour in the mean mass density profile is expected at some level as both the input galaxy stellar mass and effective radius are assumed fixed in time. Moreover, abundance matching predicts host halo masses to vary weakly at these galaxy mass scales, and this holds true either assuming a constant or slightly decreasing number density of massive galaxies up to $z \sim 1$, as anticipated in Section 3 (e.g., Shankar et al. 2006; Moster et al. 2013; Shankar et al. 2014a; Bernardi et al. 2016; Tinker et al. 2016). For instance, we checked that very similar results to those reported in Fig. 1 are obtained assuming a strictly non-evolving stellar mass-halo mass relation instead, or switching to the Moster et al. (2013) relation, both of which inherently assume some degree of evolution in the high-mass end of the stellar mass function. Assuming an ad-hoc increase in the contribution of the (flatter) dark matter distribution within the effective radius, via for example a steadily increasing AC up to $z \sim 1$ (dot-dashed, blue line), tends to induce a decrease in γ', better aligning model outputs with the strong lensing data, though still falling short in fully matching the data at $z \gtrsim 0.7$. Despite the apparent improvement, a substantial contribution of AC is in general disfavoured by the data, as emphasized in paper I and further discussed below.

At this point, despite having explored all the possible combinations of the input parameters (more relevantly IMF and host halo mass), we still fall short in reproducing the steep decline in γ' at higher redshifts. It is clear that additional assumptions/parameters are required by the data. This is a perfect example of the power and usefulness of the semi-empirical approach. The least possible assumptions and associated parameters are initially included in the models. Gradually additional degrees of complexities can be included in the model, wherever needed. This allows for ex-
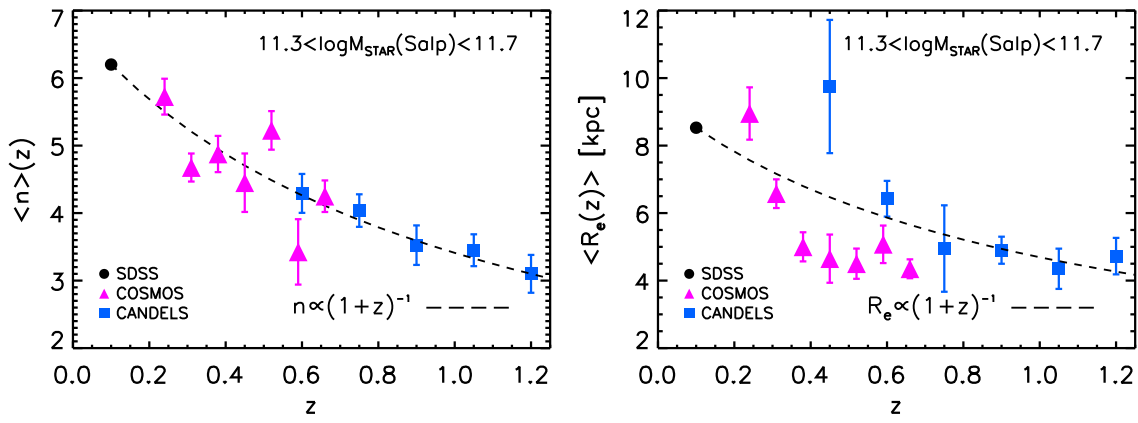
Figure 3. Measured median Sérsic index $n(z)$ (left panel) and effective radius $R_e(z)$ (right panel) as a function of redshift from COSMOS (Huertas-Company et al. 2013) and CANDELS (Huertas-Company et al. 2015), for galaxies at constant stellar mass in the range $11.3 < \log M_{star}/M_\odot < 11.7$. The filled, black circle at $z = 0.1$ is from SDSS (Bernardi et al. 2014). All the data are consistent with both quantities decreasing as $(1 + z)^{-1}$ (dashed, black lines).

treme flexibility and transparency, avoiding the risk of being clouded by an initially too heavy modelling.

In what follows, unless otherwise noted, for the stellar component we will focus on Sérsic profiles. The latter have proven to be a much more suitable model[3] to properly capture the full extent and variety of the light distribution in especially massive galaxies (e.g., Bernardi et al. 2014, and references therein). Thus we will first compute the total mass density slope γ' competing to each galaxy in our sample assuming an *intrinsic* Sérsic profile for the stellar component (and NFW for the dark matter one). However, all our predictions on γ' will continue being expressed in terms of their de Vaucouleurs counterparts in stellar mass and effective radius (available from our SDSS sample, see Section 2), to properly compare to the strong lensing observations by Sonnenfeld et al. (2013) who have always assumed a de Vaucouleurs profile. We still continue assuming that all half-mass radii (for *both* the assumed intrinsic and observed stellar profiles) evolve as $\propto (1 + z)^{-1}$.

Fig. 2 compares the predictions of a variety of models with intrinsic Sérsic stellar profiles and de Vaucouleurs stellar masses and effective radii within the intervals $11.4 < \log M_{star} < 11.6$ and $4 < R_e/\mathrm{kpc} < 6$ at $z \leqslant 0.1$, respectively, as in the observations (grey bands). These types of light profiles effectively add a degree of freedom to our semi-empirical models, namely the Sérsic index n. As shown in Appendix B of paper I, increasing n at fixed stellar mass and size produces an overall steeper stellar profile and thus naturally induces a larger total mass density slope γ'. Irrespective of the amount of adiabatic contraction, the models characterized by a constant Sérsic index n with time (black solid and purple dotted lines in the left panel), inevitably predict a more or less steep dependence of γ' on redshift, at vari-

ance with the data but in line with Fig. 1. This would hold irrespective of the choice of (time-independent) IMF, which would simply shift the black line vertically but without erasing its strong dependence on redshift (see also Fig. 1).

Assuming instead a decrease of the Sérsic index with increasing redshift, as $n \propto (1+z)^{-1}$, tends to flatten the stellar profile at fixed stellar mass and effective radius, thus inducing an overall lower γ'. The latter behavior holds irrespective of the input IMF, Salpeter, variable in velocity dispersion, variable in velocity dispersion and redshift, scale-dependent, Chabrier (blue dot-dashed, orange triple dot-dashed, green dashed, magenta dot-dashed, and red long-dashed lines, in the left panel of Fig. 2). A scale-dependent IMF, in particular, yields a significantly steeper γ' with respect to the data, even in the presence of maximal AC, which, we verified would simply reduce γ' by $\sim 25\%$. This behaviour is expected given that the stellar profile gets more prominent in the inner regions (equation 5).

The right panel of Fig. 2 shows instead the same model with velocity dispersion-dependent IMF, and different degrees of evolution in the Sérsic index with redshift, $n \propto (1 + z)^{-\delta}$. A $\delta \sim 0.5$ model is already sufficient to fully erase the dependence of γ' on redshift (dotted, orange line), while any stronger dependence characterized by $\delta \gtrsim 0.7$ can reverse the trend of γ' with redshift. On the other hand, too strong variations of the Sérsic index with time beyond $\delta \gtrsim 1.2$, tend to be disfavoured by the data, at least when the selection is made at fixed stellar mass (but see also Section 5.3). All in all, we conclude that a substantial variation in the Sérsic index with redshift of the type $n \propto (1 + z)^{-\delta}$, with $0.5 \lesssim \delta \lesssim 1.2$, is a necessary condition to align models with the strong lensing data examined in this work.

On the observational side, the issue of the structural evolution of massive galaxies in terms of size, Sérsic index and (central) surface mass density has been a subject of hot debate in the last years (e.g., Ascaso et al. 2014). At both fixed stellar mass or cumulative number density, effective radii and Sérsic indices have been claimed to evolve with redshift (e.g., van Dokkum et al. 2010; Morishita et al. 2014; Huertas-Company et al. 2015). In Fig. 3 we show the Sérsic indices n (left) and effective radii R_e (right) of galax-

---

[3] More specifically, Bernardi et al. (2014) have shown that a Sérsic+Exponential profile is the most appropriate light profile model for SDSS galaxies. However, the latter is not ideally suited to compute total mass density profiles as given by equation 6 which strictly assumes spherical symmetry. The disc component is anyway relatively small in the stellar mass scale of galaxies of interest here.
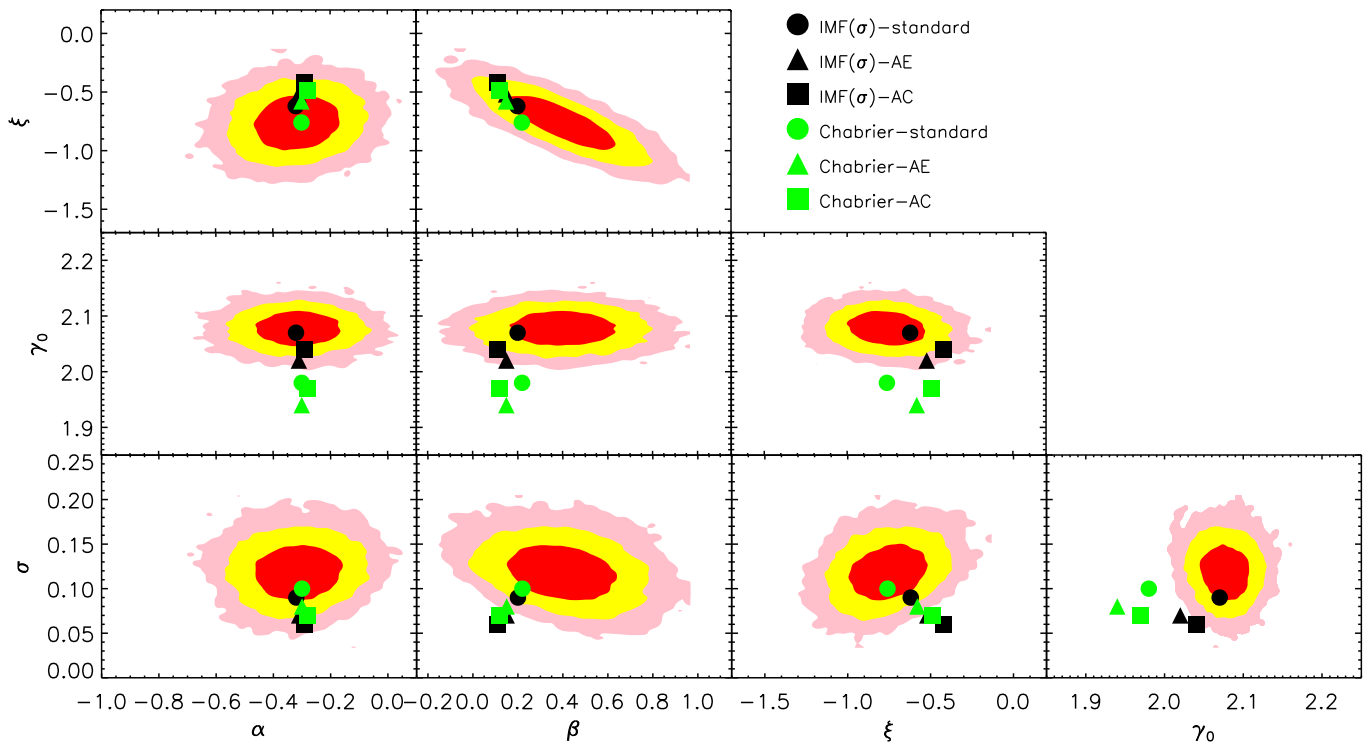
Figure 4. Covariances of posterior probability distributions of pairs of model parameters of equation 1. The red, yellow, and pink regions mark the 1σ, 2σ, and 3σ contour levels for each pair of the parameter space extracted from the Sonnenfeld et al. (2013) data. The data are compared with the predictions from the semi-empirical models based on a variable (equation 3) and Chabrier Initial Mass Functions (black and green symbols, respectively). The circles, triangles, and squares refer, respectively, to models with standard profiles, with adiabatic expansion, and with adiabatic contraction, as labelled.

ies with stellar mass $11.3 < M_{\rm star}/M_\odot < 11.7$. The latter are extracted from three (independent) galaxy samples, SDSS, COSMOS, and CANDELS, at broadly complementary redshift intervals $z < 0.3$, $0.3 < z < 1$, and $z > 0.5$, respectively, as measured by Bernardi et al. (2017b), Huertas-Company et al. (2013), and Huertas-Company et al. (2015). When taken as a whole, the data tend to suggest a relatively strong evolution of both the median n and R_e with redshift, consistent with $\propto (1 + z)^{-1}$. Note that the observed redshift evolution in effective radius and Sérsic index at fixed stellar mass reported in Fig. 3 is expected to be contributed by different galaxies at different epochs, thus the actual evolution along the single galaxies may be even stronger (see discussion and references in Section 5.3). Also, due to the limited statistical range in the observational samples, the selections in Fig. 3 are performed at fixed stellar mass *without* any cut in effective radius, as instead applied in Figs. 1 and 2. However, we have carefully checked that considering redshift evolution only at fixed stellar mass in the Sonnenfeld et al. (2013) data would, if anything, induce an even stronger flattening of γ' with redshift, strengthening our conclusions on the necessity for a strong increase of the Sérsic index with cosmic time. A varying Sérsic index with redshift for the most massive galaxies has not been fully confirmed by all observational groups. For example, Ascaso et al. (2014) find that n only mildly increases from $z = 0.9$ to $z = 0.1$. However, it is possible to ascribe these apparently contrasting results to selections of different galaxy morphological types (see, e.g., Huertas-Company et al. 2015).

We conclude this Section emphasizing that we have tested a number of physically and/or empirically motivated alterations to the reference semi-empirical models presented above. For example, we have attempted to include an increasing gas fraction associated to the central galaxy back with cosmic time, as suggested by the data compilation of Stewart et al. (2009). We have assumed that the gas follows an exponential profile with half-mass radius twice the effective radius (e.g., Guo et al. 2011, and references therein). The resulting impact on γ' is negligible, mainly because the gas fractions competing to massive galaxies is overall quite low (e.g., Stewart et al. 2009).

4.2 Probing variations in the stellar Initial Mass Function

In Section 4.1 we have highlighted that irrespective of the input stellar IMF, host halo mass, or even halo mass profile, a redshift-dependent Sérsic index is an essential component to induce a steep decrease in γ' with increasing redshift, in line with observations. In this Section we specifically focus on the stellar IMF.

It is apparent from both Figs. 1 and 2, that at $z \lesssim 0.1$ a Chabrier IMF (long-dashed, red lines) tends to be disfavoured with respect to more bottom-heavy IMFs, in line with paper I. This is more quantitatively outlined in Fig. 4 which reports the covariances on the parameters of equation 1, measured by Sonnenfeld et al. (2013). The red, yellow, and pink regions bracket, respectively, the 1σ, 2σ, and
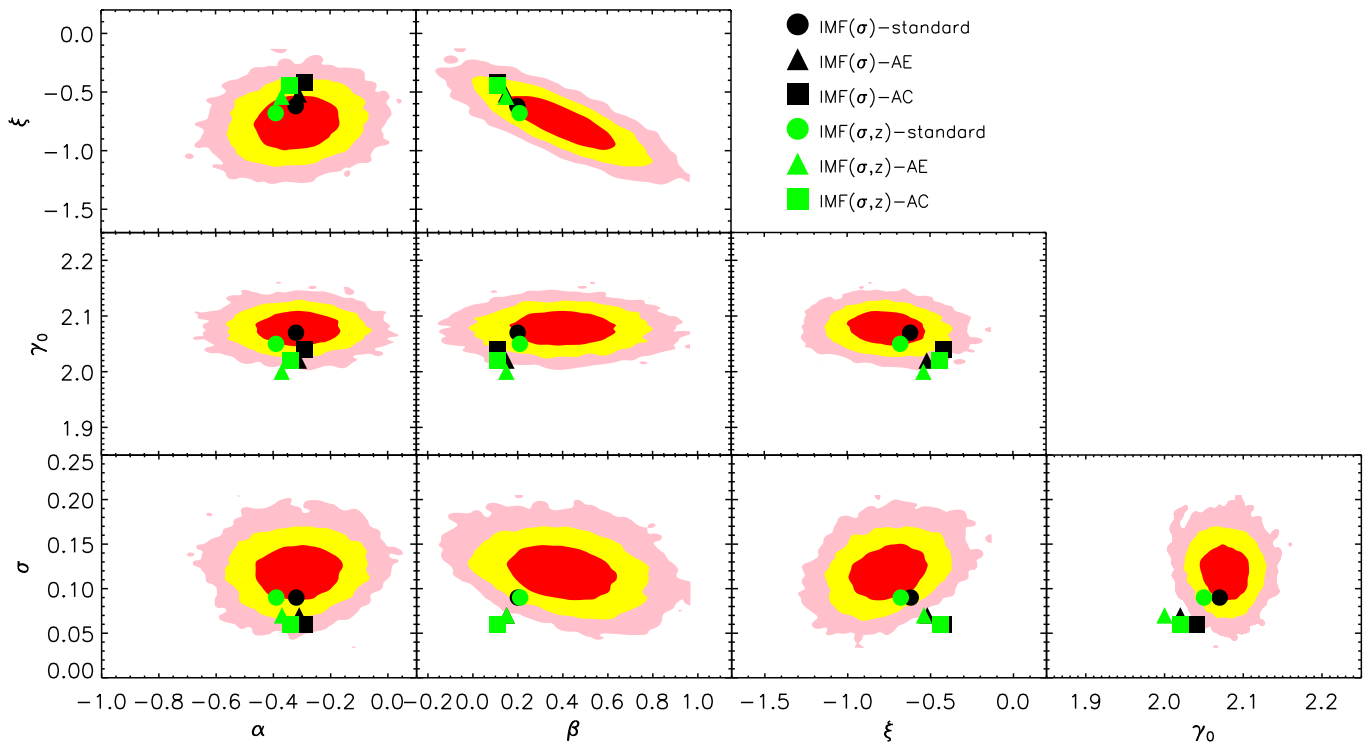
Figure 5. Similar format to Fig. 4. The red, yellow, and pink regions mark the 1σ, 2σ, and 3σ contour levels for each pair of the parameter space extracted from the Sonnenfeld et al. (2013) data (equation 1). The data are compared with the predictions from the semi-empirical models based on a IMF variable with velocity dispersion (equation 3) and a IMF variable in both velocity dispersion *and* redshift (equation 4; black and green symbols, respectively). The circles, triangles, and squares refer, respectively, to models with standard profiles, with adiabatic expansion, and with adiabatic contraction, as labelled.

3σ contour levels for each pair of the four parameters ξ, α, β, γ_0, and $\sigma_{\gamma'}$. Following paper I, we apply the same fitting procedure used in Sonnenfeld et al. (2013), modelling each of our mock galaxy samples as a Gaussian distribution with a mean given by equation 1 and with dispersion $\sigma_{\gamma'}$. The fit produces a posterior probability distribution function for the parameters γ_0, α, β, ξ and $\sigma_{\gamma'}$. For each model realization we plot the peak of the posterior probability distribution function in Fig. 4. The circles, triangles, and squares refer, respectively, to models with standard profiles, with adiabatic expansion, and with adiabatic contraction, as labelled.

Fig. 4 confirms the results of paper I: even on the assumption of a Sérsic *intrinsic* stellar profile and de Vaucouleurs as "observed" profile, a Chabrier IMF continues to be highly disfavoured with respect to a more bottom-heavy IMF, such as the variable one given in equation 3. Uncontracted NFW dark matter profiles also continue being highly preferred by the data. Adiabatic contraction tends in fact most notably to decrease β, weakening the dependence on stellar mass, and also to appreciably decrease the intrinsic scatter σ. Adiabatic expansion (black triangles) tends instead to progressively lower the dark matter contribution in the inner regions allowing for a more dominant role of the steeper stellar component, thus increasing the zero point γ_0, increasing β, and decreasing ξ.

Even more interestingly, as hinted at in Section 4.1, a Chabrier IMF seems gradually more in line with the data at $z \gtrsim 0.7$ (long-dashed, red line in Fig. 5). We quantify this trend in Fig. 5. In the specific, we here compare two models,

a variable IMF as given in equation 3 constant in time (black symbols), and a model characterized by an IMF variable in both velocity dispersion and time as in equation 4. Fig. 5 clearly shows that, while the data may continue disfavouring adiabatic contraction and expansion, at present they cannot distinguish between a time-constant or time-variable IMF, being both consistent at the $\sim 1\sigma$ level in the full space of parameters.

There are currently few measurements of the evolution in the stellar IMF that we can compare our model to. Shetty & Cappellari (2014) used stellar dynamics to put an upper limit on the IMF of a sample of 68 massive galaxies at $z \sim 0.8$, finding that, on average, the IMF cannot be heavier than a Salpeter IMF. Sonnenfeld et al. (2015) used strong lensing and stellar kinematics to constrain the evolution in the stellar IMF normalization of the lenses in the Sonnenfeld et al. (2013) sample. They found a slight preference for an IMF that becomes heavier with time (parameter ζ_{IMF} in Sonnenfeld et al. 2015). Martín-Navarro et al. (2015b) constrained the IMF slope of a set of 48 massive galaxies at $0.9 < z < 1.5$ using spectroscopic measurements of absorption lines sensitive to the abundance of low-mass stars. They found similar IMF slopes compared to samples of galaxies at $z \sim 0$. All in all, current data may still not be sufficient enough to constrain the degree of evolution in the stellar IMF along cosmic time.

A possible way to break this degeneracy could rely on probing the evolution in the normalization of the Faber-Jackson relation (e.g., Faber & Jackson 1976) and/or of the

fundamental plane of early-type galaxies (e.g., Dressler et al. 1987). As discussed by a number of groups (e.g., Prugniel & Simien 1997; Borriello et al. 2003; Mamon & Łokas 2005a,b), the central velocity dispersion σ of ellipticals is heavily dominated by the stellar component. For a one-component (stars only) spherical isotropic galaxy model with Sérsic profile, the virial theorem can be written as $GM_{\rm star}/R_e = K(n)\sigma^2$, where $K(n)$ is a dimensionless coefficient depending only on the Sérsic index n. Taking into account that massive, bulge-dominated SDSS galaxies approximately follow $M_{\rm star} \propto \sigma^2$ for $\sigma \gtrsim 100$ km/s (e.g., Barausse et al. 2017; Shankar et al. 2017a), one can then express the ratio $M_{\rm star}/\sigma^2$ as

$$\frac{M_{\rm star}}{\sigma^2} \propto K(n[z])R_e(z)\,. \qquad (7)$$

Assuming that the Sérsic index evolves with redshift as $n[z] \propto (1+z)^{-1}$, it would imply a decrease from $n \sim 6$ to $n \sim 3$ from $z \sim 0$ to $z \sim 1$ for the galaxies of interest here, according to what reported in the left panel of Fig. 3. Table 4 in Prugniel & Simien (e.g., 1997) shows that $K(n)$ would increase from $K(n) \sim 3$ when $n \sim 3$, to $K(n) \sim 5.8$ when $n \sim 6$, implying a growth with redshift $K(n[z]) \propto (1+z)^{0.96}$ which would balance the decrease in redshift of the effective radius, $R_e \propto (1+z)^{-1}$ (right panel of Fig. 3) making the ratio $M_{\rm star}/\sigma^2$ about constant in time *if* there is no additional time-evolution in $M_{\rm star}/L$.

Fig. 6 shows the velocity dispersion-stellar mass relation for our SDSS sample of galaxies. Velocity dispersions are rescaled to a circular aperture of radius equal to half of the effective radius $\sigma_{\rm e/2}$. The long dashed orange and solid black lines refer to the de Vaucouleurs and Sérsic stellar masses, respectively. The SDSS results are compared to the $z < 0.2$ and $z > 0.7$ Sonnenfeld et al. (2013) data, shown as blue squares and red circles, respectively. The Sonnenfeld et al. (2013) data do not show any evident redshift evolution in the $\sigma(R_e/2) - M_{\rm star}$ plane. The slight offset between the SDSS and the Sonnenfeld et al. (2013) data has already been noted in paper I. As discussed there, a substantial part of the offset is most probably arising from a combination of a ~ 0.1 dex higher mass-to-light ratios and larger apertures (larger effective radii) adopted by Bernardi et al. (2013) and Bernardi et al. (2017b) with respect to previous works (Hyde & Bernardi 2009). Indeed, Auger et al. (2010, see also Treu et al. 2006) did not find any noticeable offset between SLACS and Hyde & Bernardi (2009). Nevertheless, one could still conceive the presence of some selection effects in strong lensing-selected early-type galaxies, being for example more compact at fixed stellar mass. We verified, however, that by selecting in our SDSS-based mocks only those galaxies above the median σ-$M_{\rm star}$ in Fig. 6, our predictions are unchanged, as expected given that at any redshift we are selecting galaxies at fixed stellar mass and effective radius.

Recent work by Shetty & Cappellari (2015, see also, e.g., Shetty & Cappellari 2014) has also shown the $\sigma(R_e) - M(<R_e)$ relation to be constant up to $z \sim 1$ for galaxies with (dynamical) mass above $M(<R_e) > 2\times 10^{11}\ M_\odot$. Beifiori et al. (2017, and references therein) analysing 19 intermediate-mass red-sequence galaxies at $z \sim 1.5$ from the KMOS Cluster Survey, on the other hand found evidence for some evolution in the $\sigma(R_e) - M(<R_e)$ relation since $z \sim 0$. Clearly the relative roles of the $M_{\rm star}/L$ ratio against, e.g., dark matter fraction, structure, non-homology, or anisotropy in shaping
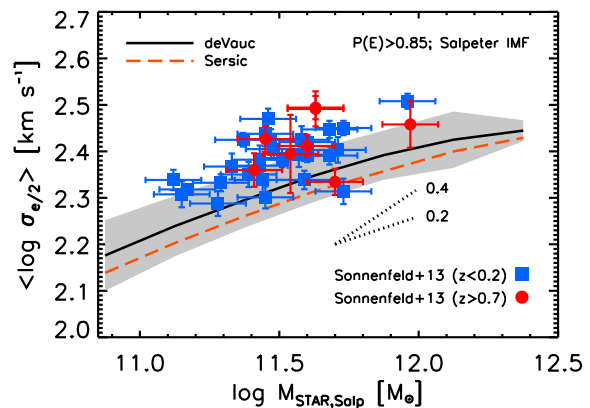

Figure 6. Line-of-sight velocity dispersion averaged within a circular aperture of radius equal to half of the effective radius $\sigma_{\rm e/2}$ as a function of (Salpeter) stellar mass for for our sample of SDSS galaxies, assuming a de Vaucouleurs (red long-dashed line) and Sérsic (black solid line) light profiles. The grey shaded region marks the 1σ dispersion around the de Vaucouleurs curve. The blue squares and red circles are, respectively, the $z < 0.2$ and $z > 0.7$ Sonnenfeld et al. (2013) data points. There is no apparent segregation between the latter two subsamples.

the massive end of the $\sigma - M_{\rm star}$ relation at different cosmic epochs are still debated. More detailed and focused modelling, which is beyond the scope of the present paper, will further discuss this and other related issues in separate work (Shankar et al. in prep.). Irrespective of all of the above, an increasingly lighter IMF at higher redshifts would be anyway insufficient, by itself, to explain the flattening of γ' at earlier epochs (see Fig. 2).

4.3 Dark Matter fractions as a function of redshift

For completeness, in Fig. 7 we present the predictions for the redshift evolution of the *projected* dark matter fraction $f_{\rm DM}(<R) = M_{\rm halo}(<R)/[M_{\rm star}(<R) + M_{\rm halo}(<R)]$ computed at the (de Vaucouleurs) effective radius $R_{\rm e,deVauc}$. At all redshifts we then compare the select in our mock catalogues galaxies with (de Vaucouleurs) stellar mass $11.4 < \log M_{\rm star}/M_\odot < 11.6$ and effective radius $4 < R_e/{\rm kpc} < 6$, fixed with redshift.

Dark matter fractions for the Sonnenfeld et al. (2013) sample of lenses have been measured by Sonnenfeld et al. (2015). These measurements have been obtained by fitting two component (bulge+halo) models to the observed Einstein radius and stellar velocity dispersion, i.e., the same data used to measure the total density slope γ'. Sonnenfeld et al. (2015) made the following assumptions: isotropic orbits, spherical symmetry, a dark matter distribution following an NFW profile with scale radius fixed to ten times the effective radius, and a stellar distribution following a spherically-deprojected de Vaucouleurs profile with a constant mass-to-light ratio. For consistency, we compare these measurements with models with fixed $n = 4$ at all redshifts.

As Fig. 7 shows, the model predicts a more or less constant dark matter fraction with time, while the data indicate an increase of dark matter fractions at higher redshift. This
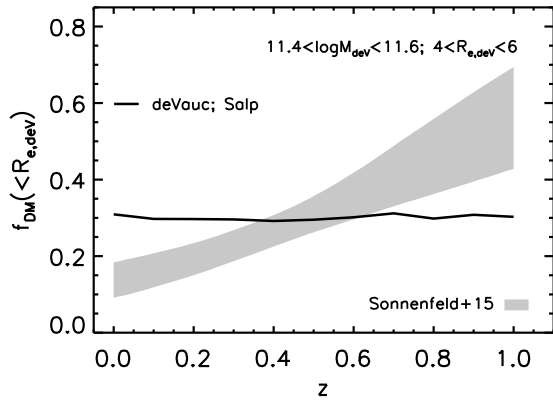
Figure 7. Predicted projected dark matter fractions within the effective radius as a function of redshift for galaxies with (de Vaucouleurs) stellar mass $11.4 < \log M_{\rm star}/M_\odot < 11.6$ and effective radius $4 < R_e/{\rm kpc} < 6$. The grey band are measurements for galaxies in the same interval of mass extracted from Sonnenfeld et al. (2015) sample, assuming NFW and de Vaucouleurs profiles for the dark matter and the stellar components, respectively. The model fails in properly reproducing the redshift increase of the dark matter fraction.

suggests that a model with a fixed de Vaucouleurs profile may not be a good description of reality, as the comparison with the evolution in γ' already suggested.

It is however important to realize that the determination of γ' is a much more robust measurement than $f_{\rm DM}$. The former has in fact a very mild dependence on the assumed stellar profile being determined by fitting a power-law density profile to the observed velocity dispersion and Einstein radius. Varying the stellar density profile has thus only a mild effect on the inference, since it only affects the distribution of the kinematical tracers, which has a small effect on the model velocity dispersion. On the other hand, modifying the stellar profile has a much more significant impact on the measurements of $f_{\rm DM}(< R)$, because it also changes the distribution of mass of the model, greatly affecting both the velocity dispersion and the Einstein radius.

The specific choice of host halo mass in the mocks clearly plays a substantial role in the predicted $f_{\rm DM}(< R)$. For example, we have verified that assuming at $z \lesssim 0.1$ a host halo mass a factor of $\lesssim 3$ lower than the one currently adopted in our reference mocks, and gradually increasing at higher redshifts, tends to improve the match to the data. A lower value of the host halo mass in the local Universe may be accounted for by a substantially steeper $M_{\rm star} - M_{\rm halo}$ relation, as recently suggested by the dynamical modelling in SDSS galaxies by (Bernardi et al. 2017a, see also Shankar et al. 2006). Irrespective of this, we have verified that including in the de Vaucouleurs, Salpeter model (solid line in Fig. 1) a varying host halo mass as the one required to align the model with the Sonnenfeld et al. (2015) $f_{\rm DM}(< R)$, would imply a $\gamma' \sim 2.20$ at $z \lesssim 0.1$ gradually increasing to $\gamma' \sim 2.24$ at $z \sim 1$, still much steeper than what suggested by the strong lensing data for which $\gamma' \sim 2.05 \pm 0.08$ at $z \sim 1$ (grey area in Fig. 1).

5 DISCUSSION

5.1 Impact of observational selection effects

The main point emphasized in Section 4 is that semi-empirical models struggle to reproduce the apparent increase of γ' as a function of cosmic time, *unless* the Sérsic index n is allowed to strongly vary as $\propto (1+z)^\delta$, with $\delta \lesssim -1$. To set these conclusions on a firmer foot, it is important to properly understand whether some selection effects may be biasing the apparent redshift evolution of γ' and in turn our physical interpretation of the observational data.

The main effect of strong lensing selection on a sample of galaxies is to skew its distribution towards a region of parameter space corresponding to galaxies with a higher strong lensing cross-section. This can in principle alter the distribution in γ' of a sample of strong lenses compared to that of the general population of galaxies. To assess the importance of this effect, we carry out the following experiment. For each galaxy in our mock, we calculate its strong lensing cross-section, i.e., the area enclosed within its radial caustic in the source plane, assuming spherical symmetry. This requires assuming a source redshift, z_s. We fix $z_s = 0.6$ for galaxies at redshift $z < 0.3$ and $z_s = 2$ for galaxies at a higher redshift, to mimic the source redshift distribution of SLACS and SL2S lenses, on which the Sonnenfeld et al. (2013) measurements are based. We then draw a subset of 10,000 objects from the mock, weighting each object by its strong lensing cross-section. This subsample is intended to resemble a set of strong lensing-selected objects. Finally, we fit our model distribution of γ' to this mock strong lens sample and compare it with the result obtained over the whole sample.

Our results are reported in Fig. . The latter compares the Sonnenfeld et al. (2013) 1σ, 2σ, and 3σ contour levels of the posterior probability of each data pair in equation 6, with the predictions from our reference semi-empirical models based on a IMF variable with velocity dispersion (equation 3), and a variable $n \propto (1 + z)^{-1}$ Sérsic index, inclusive (green triangles) or not (black circles) of strong lensing selection effects. We find small differences. The more relevant effect is a ~ 0.03 increase in the average slope, γ_0' but with virtually no effect on its dependence on redshift, i.e., on α. This is well understood, as galaxies with a steeper density profile have a larger lensing cross-section. However, the shift with respect to the distribution of the whole sample is small, owing to the relatively small scatter in γ'. For completeness, in the same Fig. we also include the results of the model with a constant Sérsic index. The latter naturally predicts (blue squares) a null evolution in redshift, thus $\alpha \approx 0$, and thus a much larger value of γ_0'. Including the above-quoted strong lensing selection effects (magenta stars) if anything further worsens the match to the data, further strengthening our conclusions on the need for a strong evolving Sérsic index.

Xu et al. (2017), have also stressed that additional systematics in the comparison between models and data could arise from varying degrees of stellar anisotropy, which should anyhow be limited to differences of $\lesssim 0.1$ in γ' between $z = 0$ and $z = 1$, comparable to, or even smaller than, current observational uncertainties.
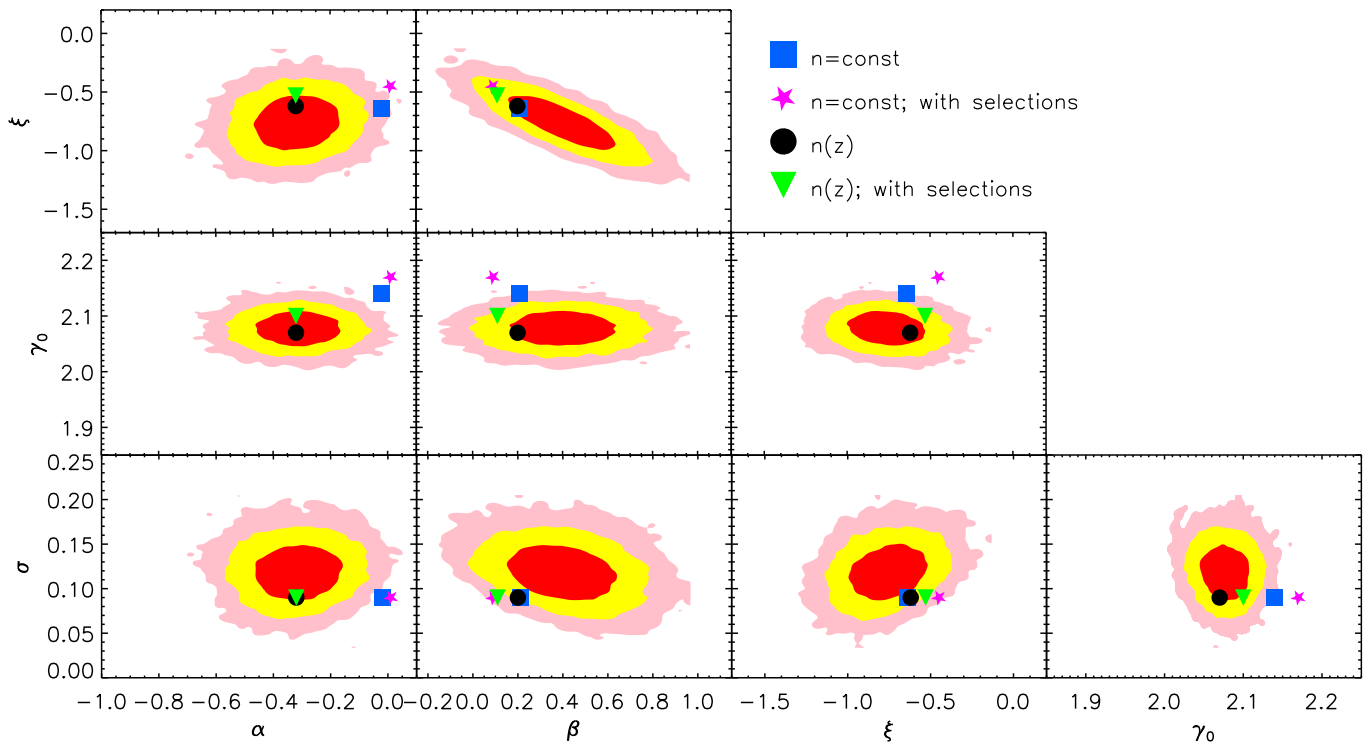
Figure 8. Similar format to Fig. 4. The red, yellow, and pink regions mark the 1σ, 2σ, and 3σ contour levels for each pair of the parameter space extracted from the Sonnenfeld et al. (2013) data (equation 1). The data are compared with predictions from the semi-empirical models based on a IMF variable with velocity dispersion (equation 3), and, as labelled, a constant Sérsic index with (magenta stars) and without (blue squares) strong lensing observational selection effects, and a redshift-dependent Sérsic index with (green triangles) and without (black circles) strong lensing observational selection effects. See text for details.

5.2 Comparison with Semi Analytic Models

Up to this point we have compared available data with basic semi-empirical models to minimize the number of input parameters and assumptions, thus allowing for a more transparent and secure interpretation of the data. We have also calculated the redshift evolution in the total mass density profiles of massive galaxies extracted from the Guo et al. (2011) semi-analytic model. To this purpose we used their publicly available online catalogues[4] with stellar and halo masses, and applied the same virial radii, halo profiles, and concentrations as in our reference models. We also compared with the Shankar et al. (2013) variant of the Guo et al. (2011), which includes gas dissipation in major mergers and parabolic orbital energies.

Analogously to our mocks, we find these semi-analytic models to predict for bulge-dominated, massive galaxies a steeper evolution of γ' out to $z \sim 1$ with respect to the Sonnenfeld et al. (2013) data. In line with our previous findings, modelling galaxy profiles as Sérsic with redshift-dependent Sérsic index n provides an improved match to the data.

5.3 Evolution along the "progenitors"

So far we have always discussed structural evolution at *fixed* stellar mass and size. This may not help us to distinguish among different evolutionary scenarios. In fact, the impact

---

[4] http://www.g-vo.org/MyMillennium3

of new galaxies entering the selection at later epochs may substantially contribute to the observed structural evolution of massive galaxies (e.g., Cimatti et al. 2012; Carollo et al. 2013; Shankar et al. 2015, and references therein), the so-called "progenitor bias" effect (e.g., van Dokkum & Franx 1996; Saglia et al. 2010). So, what would be the evolution of the total mass density profiles along the "progenitors"? Of course, the galaxy stellar mass is expected to be lower in the progenitors, possibly inducing flatter γ' values.

It is clearly observationally challenging to identify galaxy progenitors along cosmic time. A number of techniques have been proposed in the last decade to achieve this goal, most notably number density conservation (e.g., van Dokkum et al. 2010; Patel et al. 2013; Huertas-Company et al. 2015). van Dokkum et al. (2010), in particular, suggest that massive galaxies, in the range of stellar mass of interest here, should decrease in mass at earlier redshifts as

$$\log M_{\rm star}[z] = \log M_{\rm star}[z=0] - 0.67\log(1+z). \quad (8)$$

This would imply progenitors ~ 0.2 dex lower at $z \sim 1$, in broad agreement with other independent observationally-driven studies (e.g., Lidman et al. 2012; Vulcani et al. 2016), and semi-empirical modelling (e.g., Shankar et al. 2014b, 2015).

We start with SDSS galaxies in our sample with $\log M_{\rm star} \sim 11.5$ (Salpeter), characterized by median (de Vaucouleurs) effective radii of $R_e \sim 8$ kpc. We then evolve these galaxies back to $z = 1$, assuming an evolution in stellar mass as given by equation 8 and in effective radius of

$\propto (1+z)^{-1}$. For these "progenitor" galaxies the resulting total mass density slope is $\gamma' = 2.03 \pm 0.08$, adopting the posterior probability distribution by Sonnenfeld et al. (2013) data and equation 6. Our reference semi-empirical model with intrinsic Sérsic profile and observed de Vaucouleurs for the stellar component, with a redshift evolution in both the Sérsic effective radius and Sérsic index as $\propto (1+z)^{-1}$, would predict for the same set of progenitor galaxies $\gamma' \sim 2.00$, in full agreement with what inferred from the strong lensing posterior probability distribution. On the other hand, assuming no evolution in the Sérsic index would yield $\gamma' = 2.31$, more than $\gtrsim 3\sigma$ away from the strong lensing data. A strong evolution in the Sérsic index thus seems to remain a necessary condition in evolving the single galaxies, and not a simple byproduct of progenitor bias effects.

But how can the Sérsic index evolve so strongly with cosmic time? An increase with Sérsic index has been suggested as a consequence of mergers. Hopkins et al. (2009) suggested that at each merger event the Sérsic index should increase by an amount

$$\Delta n \sim k \left(\frac{\Delta M}{M_{\mathrm{cen}}} \right) \qquad (9)$$

where k is a constant and ΔM is the amount of stellar mass increase in the central galaxy M_{cen} after a merger. Hopkins et al. (2009) suggested that $k \sim 1$, while Hilz et al. (2013) found that for galaxies embedded in dark matter haloes, minor mergers induce a significantly faster size growth and profile reshaping with respect to galaxies without dark matter (see also Nipoti et al. 2003). Forcing equation 9 to broadly match the Hilz et al. (2013) numerical simulations (their Fig. 5), would roughly correspond to $k \sim 2-3$ for major mergers and $k \sim 5-20$ for minor mergers, which would imply an increase of Sérsic index of up to five units for a stellar mass growth of just a factor ~ 1.6 (solid, red line in their Fig. 5). It is highly unclear whether any of the latter proposed solutions will be able to yield an increase in Sérsic index as strong and sharp as the one actually observed (Fig. 3). A close inspection of this important issue is beyond the scope of this paper and it will be explored in future work.

5.4 Comparison to previous work on the topic

One of the most novel results of this work is the interpretation of the redshift evolution of γ'. The observed evolution of a decreasing γ' at increasingly higher redshifts, cannot simply be due to only selection effects (e.g., Sonnenfeld et al. 2013, 2015) or systematic measurement errors. Independent observations point to a similar, if not stronger, flattening of γ' with increasing redshift (e.g., Dye et al. 2014; Morishita et al. 2014). Previous observational work also inferred a less or equally significant flattening of the total mass density profiles back in cosmic time (Koopmans et al. 2006; Ruff et al. 2011; Bolton et al. 2012).

Ruff et al. (2011) suggested that dissipative processes might have played some role in the growth of massive galaxies and the steepening of the mass profile since $z \sim 1$. Bolton et al. (2012) noted that significant baryonic dissipation at late times is in contrast with the very low star formation rate and old stellar populations characterizing massive, early-type galaxies. Inspired by the numerical simulations of

Nipoti et al. (2009), they instead pointed out the possibility that off-axis major dry mergers could contribute towards the observed evolution in γ'.

However, purely dry mergers have been disfavoured by Sonnenfeld et al. (2014) as a viable mechanism for the observed trend of γ' with redshift, as they pointed out that such mergers produce a flattening of the density slope with time, once cosmologically motivated stellar-to-halo mass ratios and self-consistent definitions of γ' between simulations and observations are used. Sonnenfeld et al. (2014) suggested that mergers with small amounts of dissipation and nuclear star formation (consistent with observational constraints) are required to fit the lensing data.

Cosmological hydro-simulations dedicated to the full study of the evolution of massive, early-type galaxies, have also been used to made predictions on the evolution of the density slope. Dubois et al. (2013) find an average γ' that becomes steeper with time, in agreement with the data. Johansson et al. (2012), on the other hand, find a nearly flat evolution for the total logarithmic density slope below $z \lesssim 1$, and steeply rising above $z \sim 1$.

Xu et al. (2017) have recently carefully analyzed the total mass density slopes of early-type galaxies in the Illustris simulation finding a mild increase towards lower redshifts, in broad agreement with the data.

Remus et al. (2017) further extended their previous analysis (Remus et al. 2013) presenting evidence from their cosmological hydrodynamical simulations that the dark matter fraction within the half-mass radius is lower at higher redshifts, in line with what discussed here and the obervationally-oriented results by Tortora et al. (2014b). On the other hand, they find their total mass density slopes γ to behave in stark contrast to observations, predicting steeper slopes at higher redshifts. They claim this discrepancy between observations and simulations to be mostly a result of the observational methodology adopted to determine the density slopes. In our semi-empirical models we do not find evidence for such strong tensions with the data. Indeed, at fixed stellar mass and effective radius our γ' slopes are already predicted to be roughly constant with redshift. Once accounting for a Sérsic index evolution as suggested by independent observations, the γ' are then predicted to naturally steepen with cosmic time, in nice agreement with Sonnenfeld et al. (2013).

6 CONCLUSIONS

In this second paper of the series we carry out a systematic investigation of the total mass density profile of massive ($\log M_{\mathrm{star}}/M_{\odot} \sim 11.5$) early-type galaxies and its dependence on redshift, specifically in the range $0 \lesssim z \lesssim 1$. We start from a large sample of SDSS early-type galaxies with measured stellar masses and effective radii assuming two different intrinsic profiles, de Vaucouleurs and Sérsic. Via abundance matching relations we assign to galaxies dark matter haloes with standard ΛCDM profiles and concentrations. We then compute the total, mass-weighted density slope at the effective radius γ', and study its redshift dependence at fixed stellar mass and effective radius. We find that a necessary condition to induce an increasingly flatter γ' at higher redshifts, as suggested by current strong lensing

data, is to allow the intrinsic stellar profile of massive galaxies to be Sérsic and the input Sérsic index n to vary with redshift as $n(z) \propto (1 + z)^{\delta}$, with $\delta \lesssim -1$. This conclusion holds irrespective of the input M_{star}-M_{halo} relation, the assumed stellar initial mass function, or even the chosen level of adiabatic contraction in the model. Secondary contributors to the observed redshift evolution of γ' may come from possible increases at earlier times in the adiabatic contraction and/or contributions from a bottom-light IMF. We have also explored the possible impact of strong lensing selection effects. The latter may induce an increase in the average slope, γ'_0, but have virtually no effect on its dependence on redshift, i.e., on the parameter α in equation 1. A steadily increasing Sérsic index with cosmic time is supported by independent observations, though it is not yet clear whether cosmological hierarchical models (e.g., mergers) are capable of reproducing such a fast and sharp evolution.

ACKNOWLEDGMENTS

REFERENCES

Abazajian K. N. et al., 2009, ApJS, 182, 543

Ascaso B., Lemaux B. C., Lubin L. M., Gal R. R., Kocevski D. D., Rumbaugh N., Squires G., 2014, MNRAS, 442, 589

Auger M. W., Treu T., Bolton A. S., Gavazzi R., Koopmans L. V. E., Marshall P. J., Moustakas L. A., Burles S., 2010, ApJ, 724, 511

Aversa R., Lapi A., de Zotti G., Shankar F., Danese L., 2015, ApJ, 810, 74

Barausse E., 2012, MNRAS, 423, 2533

Barausse E., Shankar F., Bernardi M., Dubois Y., Sheth R. K., 2017, ArXiv:1702.01762

Barnabè M., Czoske O., Koopmans L. V. E., Treu T., Bolton A. S., 2011, MNRAS, 415, 2215

Behroozi P. S., Wechsler R. H., Conroy C., 2013, ApJ, 770, 57

Beifiori A. et al., 2017, ApJ, 846, 120

Bell E. F., McIntosh D. H., Katz N., Weinberg M. D., 2003, ApJS, 149, 289

Bernardi M., Fischer J.-L., Sheth R. K., Meert A., Huertas-Company M., Shankar F., Vikram V., 2017a, ArXiv:1702.08527

Bernardi M., Meert A., Sheth R. K., Fischer J.-L., Huertas-Company M., Maraston C., Shankar F., Vikram V., 2017b, MNRAS

Bernardi M., Meert A., Sheth R. K., Huertas-Company M., Maraston C., Shankar F., Vikram V., 2016, MNRAS, 455, 4122

Bernardi M., Meert A., Sheth R. K., Vikram V., Huertas-Company M., Mei S., Shankar F., 2013, MNRAS, 436, 697

Bernardi M., Meert A., Vikram V., Huertas-Company M., Mei S., Shankar F., Sheth R. K., 2014, MNRAS, 443, 874

Bernardi M., Shankar F., Hyde J. B., Mei S., Marulli F., Sheth R. K., 2010, MNRAS, 404, 2087

Blumenthal G. R., Faber S. M., Flores R., Primack J. R., 1986, ApJ, 301, 27

Bolton A. S. et al., 2012, ApJ, 757, 82

Borriello A., Salucci P., Danese L., 2003, MNRAS, 341, 1109

Buchan S., Shankar F., 2016, MNRAS, 462, 2001

Cappellari M., 2016, ArXiv:1602.04267

Cappellari M. et al., 2015, ApJ, 804, L21

Carollo C. M. et al., 2013, ApJ, 773, 112

Chabrier G., 2003, PASP, 115, 763

Cimatti A., Nipoti C., Cassata P., 2012, MNRAS, 422, L62

Cirasuolo M., Shankar F., Granato G. L., De Zotti G., Danese L., 2005, ApJ, 629, 816

Conroy C., van Dokkum P. G., Villaume A., 2017, ApJ, 837, 166

Coupon J. et al., 2015, MNRAS, 449, 1352

De Lucia G., Blaizot J., 2007, MNRAS, 375, 2

de Vaucouleurs G., 1948, Annales d'Astrophysique, 11, 247

Dekel A., Sari R., Ceverino D., 2009, ApJ, 703, 785

Diemer B., Kravtsov A. V., 2015, ApJ, 799, 108

Dressler A., Lynden-Bell D., Burstein D., Davies R. L., Faber S. M., Terlevich R., Wegner G., 1987, ApJ, 313, 42

Dubois Y., Gavazzi R., Peirani S., Silk J., 2013, MNRAS, 433, 3297

Dutton A. A., Treu T., 2014, MNRAS, 438, 3594

Dutton A. A., van den Bosch F. C., Dekel A., Courteau S., 2007, ApJ, 654, 27

Dye S. et al., 2014, MNRAS, 440, 2013

Faber S. M., Jackson R. E., 1976, ApJ, 204, 668

Gavazzi R., Treu T., Rhodes J. D., Koopmans L. V. E., Bolton A. S., Burles S., Massey R. J., Moustakas L. A., 2007, ApJ, 667, 176

González J. E., Lacey C. G., Baugh C. M., Frenk C. S., 2011, MNRAS, 128

Guo Q. et al., 2011, MNRAS, 413, 101

Hilz M., Naab T., Ostriker J. P., 2013, MNRAS, 429, 2924

Hirschmann M., De Lucia G., Iovino A., Cucciati O., 2013, ArXiv e-prints

Hopkins P. F., Hernquist L., Cox T. J., Keres D., Wuyts S., 2009, ApJ, 691, 1424

Hopkins P. F., Hernquist L., Cox T. J., Kereš D., 2008, ApJS, 175, 356

Huertas-Company M., Aguerri J. A. L., Bernardi M., Mei S., Sánchez Almeida J., 2011, A&A, 525, A157

Huertas-Company M. et al., 2013, MNRAS, 428, 1715

Huertas-Company M. et al., 2015, ApJ, 809, 95

Hyde J. B., Bernardi M., 2009, MNRAS, 394, 1978

Johansson P. H., Naab T., Ostriker J. P., 2012, ApJ, 754, 115

Koopmans L. V. E. et al., 2009, ApJ, 703, L51

Koopmans L. V. E., Treu T., Bolton A. S., Burles S., Moustakas L. A., 2006, ApJ, 649, 599

Kravtsov A., Vikhlinin A., Meshscheryakov A., 2014, ArXiv:1401.7329

Kroupa P., 2001, MNRAS, 322, 231

La Barbera F., Vazdekis A., Ferreras I., Pasquali A., Cappellari M., Martín-Navarro I., Schönebeck F., Falcón-Barroso J., 2016, MNRAS, 457, 1468

Lapi A. et al., 2011, ApJ, 742, 24

Lapi A., Shankar F., Mao J., Granato G. L., Silva L., De Zotti G., Danese L., 2006, ApJ, 650, 42

Lidman C. et al., 2012, MNRAS, 427, 550

Mamon G. A., Łokas E. L., 2005a, MNRAS, 362, 95

Mamon G. A., Łokas E. L., 2005b, MNRAS, 363, 705

Martín-Navarro I., La Barbera F., Vazdekis A., Falcón-Barroso J., Ferreras I., 2015a, MNRAS, 447, 1033

Martín-Navarro I. et al., 2015b, ApJ, 798, L4

Martín-Navarro I. et al., 2015c, ApJ, 806, L31

Meert A., Vikram V., Bernardi M., 2015, MNRAS, 446, 3943

Mendel J. T., Simard L., Ellison S. L., Patton D. R., 2013, MNRAS, 429, 2212

Morishita T., Ichikawa T., Kajisawa M., 2014, ApJ, 785, 18

Moster B. P., Naab T., White S. D. M., 2013, MNRAS, 428, 3121

Naab T., Johansson P. H., Ostriker J. P., 2009, ApJ, 699, L178

Navarro J. F., Frenk C. S., White S. D. M., 1997, ApJ, 490, 493

Newman A. B., Ellis R. S., Treu T., 2015, ApJ, 814, 26

Newman A. B., Treu T., Ellis R. S., Sand D. J., 2013, ApJ, 765, 25

Nipoti C., Londrillo P., Ciotti L., 2003, MNRAS, 342, 501

Nipoti C., Treu T., Auger M. W., Bolton A. S., 2009, ApJ, 706, L86

Oser L., Ostriker J. P., Naab T., Johansson P. H., Burkert A., 2010, ApJ, 725, 2312

Patel S. G., Kelson D. D., Williams R. J., Mulchaey J. S., Dressler A., McCarthy P. J., Shectman S. A., 2015, ApJ, 799, L17

Patel S. G. et al., 2013, ApJ, 766, 15

Prugniel P., Simien F., 1997, A&A, 321, 111

Remus R.-S., Burkert A., Dolag K., Johansson P. H., Naab T., Oser L., Thomas J., 2013, ApJ, 766, 71

Remus R.-S., Dolag K., Naab T., Burkert A., Hirschmann M., Hoffmann T. L., Johansson P. H., 2017, MNRAS, 464, 3742

Rodríguez-Puebla A., Avila-Reese V., Yang X., Foucaud S., Drory N., Jing Y. P., 2015, ApJ, 799, 130

Ruff A. J., Gavazzi R., Marshall P. J., Treu T., Auger M. W., Brault F., 2011, ApJ, 727, 96

Saglia R. P. et al., 2010, A&A, 524, A6

Salpeter E. E., 1955, ApJ, 121, 161

Sérsic J. L., 1963, Boletin de la Asociacion Argentina de Astronomia La Plata Argentina, 6, 41

Shan Y., McDonald M., Courteau S., 2015, ApJ, 800, 122

Shankar F., Bernardi M., Sheth R. K., 2017a, MNRAS

Shankar F. et al., 2015, ApJ, 802, 73

Shankar F. et al., 2014a, ApJ, 797, L27

Shankar F., Lapi A., Salucci P., De Zotti G., Danese L., 2006, ApJ, 643, 14

Shankar F., Marulli F., Bernardi M., Boylan-Kolchin M., Dai X., Khochfar S., 2010a, MNRAS, 405, 948

Shankar F., Marulli F., Bernardi M., Dai X., Hyde J. B., Sheth R. K., 2010b, MNRAS, 403, 117

Shankar F., Marulli F., Bernardi M., Mei S., Meert A., Vikram V., 2013, MNRAS, 428, 109

Shankar F. et al., 2014b, MNRAS, 439, 3189

Shankar F. et al., 2017b, ApJ, 840, 34

Shetty S., Cappellari M., 2014, ApJ, 786, L10

Shetty S., Cappellari M., 2015, MNRAS, 454, 1332

Skibba R. A. et al., 2014, ApJ, 784, 128

Sonnenfeld A., Nipoti C., Treu T., 2014, ApJ, 786, 89

Sonnenfeld A., Nipoti C., Treu T., 2017, MNRAS, 465, 2397

Sonnenfeld A., Treu T., Gavazzi R., Suyu S. H., Marshall P. J., Auger M. W., Nipoti C., 2013, ApJ, 777, 98

Sonnenfeld A., Treu T., Marshall P. J., Suyu S. H., Gavazzi R., Auger M. W., Nipoti C., 2015, ApJ, 800, 94

Stewart K. R., Bullock J. S., Wechsler R. H., Maller A. H., 2009, ApJ, 702, 307

Tinker J., Kravtsov A. V., Klypin A., Abazajian K., Warren M., Yepes G., Gottlöber S., Holz D. E., 2008, ApJ, 688, 709

Tinker J. L. et al., 2016, ArXiv:1607.04678

Tortora C., La Barbera F., Napolitano N. R., Romanowsky A. J., Ferreras I., de Carvalho R. R., 2014a, MNRAS, 445, 115

Tortora C., Napolitano N. R., Saglia R. P., Romanowsky A. J., Covone G., Capaccioli M., 2014b, MNRAS, 445, 162

Treu T., Koopmans L. V., Bolton A. S., Burles S., Moustakas L. A., 2006, ApJ, 640, 662

Treu T., Koopmans L. V. E., 2004, ApJ, 611, 739

van der Wel A. et al., 2014, ApJ, 788, 28

van Dokkum P., Conroy C., Villaume A., Brodie J., Romanowsky A. J., 2017, ApJ, 841, 68

van Dokkum P. G., Franx M., 1996, MNRAS, 281, 985

van Dokkum P. G. et al., 2010, ApJ, 709, 1018

Vulcani B. et al., 2016, ApJ, 816, 86

Wojtak R., Mamon G. A., 2013, MNRAS, 428, 2407

Xu D., Springel V., Sluse D., Schneider P., Sonnenfeld A., Nelson D., Vogelsberger M., Hernquist L., 2017, MNRAS, 469, 1824